ARTICLE IN PRESS

Available online at www.sciencedirect.com

SCIENCE DIRECT®

Journal of Electrostatics ▮ (▮▮▮▮) ▮▮▮–▮▮▮

Journal of ELECTROSTATICS

www.elsevier.com/locate/elstat

Dispensing picoliter droplets on substrates using dielectrophoresis

R. Ahmed*, T.B. Jones

Department of Electrical and Computer Engineering, University of Rochester, Rochester, NY 14627-0126, United States

Abstract

Liquid dielectrophoresis is exploited to initiate rapid, transient flow of aqueous liquids along co-planar electrodes patterned on insulating substrates. The flow induced by the non-uniform electric field leads to a new electrostatic equilibrium. A reduced-order model predicts the transient motion of the rivulet. When the field is removed, capillary instability breaks up the rivulet into regularly spaced droplets. Periodic circular bumps patterned on the structure, when spaced according to the most unstable wavelength based on Rayleigh's inviscid theory for the cylindrical liquid jet, lead to uniformly spaced and sized droplets. A correction factor, based on the dimensionless Ohnesorge number, accounts successfully for the effect of viscosity.
© 2005 Elsevier B.V. All rights reserved.

Keywords: Dielectrophoresis; Capillary instability; Droplet dispensing; Microfluidics

1. Introduction

The dielectrophoretic (DEP) force, created by a non-uniform AC electric field and exerted on dielectrics, can be exploited using co-planar electrodes patterned on insulating substrates to move and manipulate liquid water and to dispense uniform linear arrays of very small droplets on the surface. This scheme of droplet generation has potential applications for microfluidics in lab-on-a-chip technology. The DEP force draws out a liquid finger or rivulet starting from a parent droplet when an AC voltage is applied [1]. The transient flow ultimately creates a new hydrostatic equilibrium due to the non-uniform electric field.

We present a reduced-order dynamic model that describes the motion of this finger as a function of square root of time, t. Experimental data adhere to the model reasonably well. Once the voltage is removed, the electrohydrostatic equilibrium is disrupted due to capillary instability, and the rivulet breaks up into regularly spaced droplets on the surface. Rayleigh's hydrodynamic instability theory for the cylindrical jet accurately determines the most unstable wavelength, λ^*, which controls droplet spacing and volume. Circular bumps patterned onto the co-planar electrodes and spaced at $\lambda^* = 9.016R$ control this process and lead to uniformly spaced and sized, sessile droplets.

2. Experimental

The co-planar electrode structures are typically patterned on 50 mm square borosilicate glass substrates of thickness 2 mm. A layer of aluminum 0.3–0.5 μm thick is thermally evaporated on the substrates and then co-planar electrodes are patterned using conventional photolithography. Refer to Fig. 1. The electrodes must be coated with a dielectric layer to prevent any secondary reactions, especially electrolysis, from occurring on the surface. We have used Teflon^{TM} and SU-8^{TM} as the dielectric materials. The dielectric layer requires a thin topcoat of a hydrophobic material to minimize the effects of contact angle hysteresis and stiction. This coating controls the wetting conditions of the surface by maintaining the hydrophobic nature of the surface.

To alleviate Joule heating that occurs when high voltage is applied to the electrodes, experiments are performed under a layer of insulating oil. The oil helps dissipate heat through thermal conduction across the liquid–liquid interface.

To conduct an experiment, a droplet of deionized water is dispensed at one end of the electrodes. See Fig. 1. If the voltage is sufficient, a finger of liquid in the shape of a

*Corresponding author.
E-mail address: rajib@ece.rochester.edu (R. Ahmed).

0304-3886/$ - see front matter © 2005 Elsevier B.V. All rights reserved.
doi:10.1016/j.elstat.2005.10.008

rivulet emerges from the droplet and flows down along the structure. The actuation is shown in Fig. 2. The video frames are divided into two segments, the top three depicting transient motion of the liquid finger when the voltage is on, and the bottom three showing capillary instability-driven droplet formation when the voltage is turned off. Each frame shows simultaneous side (upper) and top (lower) views of the experiment. The side view was obtained by placing a 55° mirror directly adjacent and parallel to the electrodes. The first frame shows a ~1 μL parent water droplet (conductivity $\sigma_w \sim 10^{-4}$ S/m) at the left end of the structure. The second frame shows the liquid finger moving from left to right at AC voltage of ~600 V-rms. The third frame depicts the leading edge of the finger approaching the right end of the structure.

The finger has reached the end of the structure and the flow has stopped in the fourth frame. In the fifth frame, the voltage has been turned off, capillary instability is in progress, a droplet is forming, and some of the liquid is being drawn back to the left. The sixth frame shows a completely formed sessile droplet, roughly hemispherical in shape, on the substrate. Actuation occurs very rapidly, with the rivulet reaching the end of the structure in ~120 ms and the droplet forming within 12 ms after voltage removal.

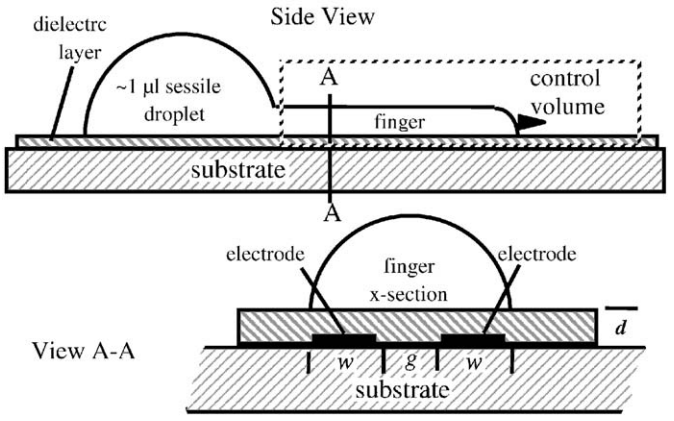

Fig. 1. Side view and cross-section (view A-A) of DEP actuation using parallel, co-planar electrodes. The motion is transient and ceases when the liquid reaches the end of the electrodes opposite the sessile droplet. The non-uniform electric field confines the footprint of the finger to a width of approximately $2w+g$, and the cross section is roughly semicircular.

3. Dynamics of finger motion

Two principal mechanisms control DEP droplet dispensing: (i) DEP-driven transient motion of the finger in response to the voltage and (ii) formation of the droplets by action of the capillary instability after removal of voltage. In both regimes, fairly simple predictive models seem to describe the observed behavior.

3.1. Model for finger dynamics

Liquid DEP is the force, attractive or repulsive, exerted on dielectric fluids by a non-uniform electric field [2,3]. The dipoles, individual molecules in the case of a liquid, respond to the field by collecting preferentially where

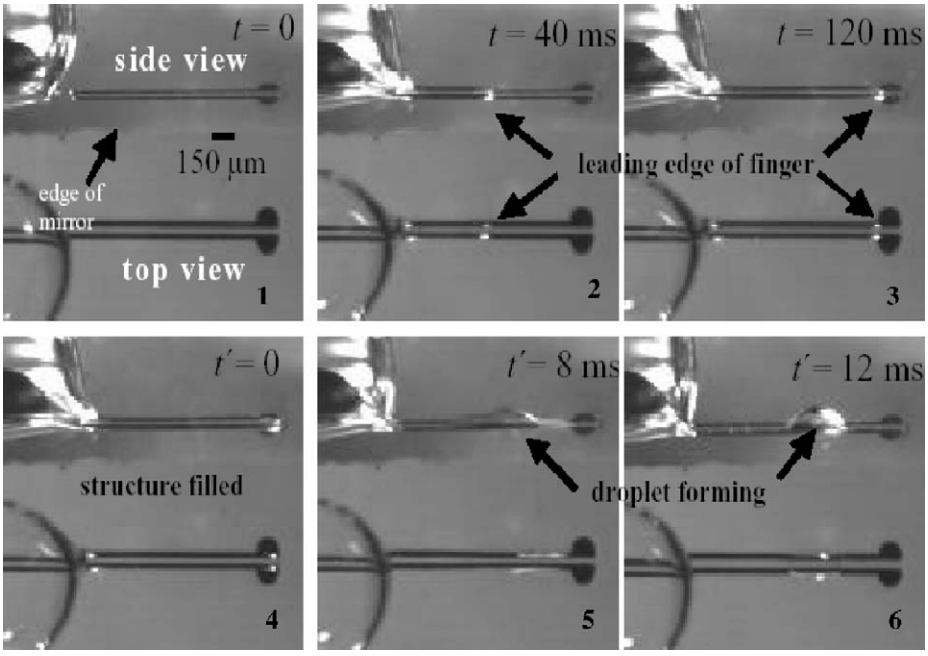

Fig 2. Frames from a video sequence taken at 250 fps showing side (using a 55° mirror) and top views of finger motion from left to right, when the voltage is turned on, and then droplet formation due to the capillary instability, when the voltage is turned off. The electrode width $w = 50$ μm, and gap $g = 50$ μm. Note the droplet shape. Droplet formation takes ~1/10 the time required for the finger to reach the end of the 3 mm long structure. (T. Ito, Toba National College of Maritime Technology, Toba, Japan, assisted in obtaining the video from which these frames were taken.)

the field intensity is highest. Thus, when the voltage is turned on, the liquid rushes to fill the roughly half-cylindrical volume between and adjacent to the inter-electrode gap.

Consider a liquid finger already emerged from a sessile droplet of length $Z(t)$ and moving along the electrodes, as shown in Fig. 1. Writing the momentum conservation expression for a control volume containing the finger yields

$$\frac{\mathrm{d}}{\mathrm{d}t}\left[(\rho A_x)Z\frac{\mathrm{d}Z}{\mathrm{d}t}\right] = f^{\mathrm{e}} + f_\gamma + f_{\mathrm{d}}, \tag{1}$$

where ρ and $A_x = (\pi/2)(w + g/2)^2$ are the fluid density and semi-circular cross-sectional area, respectively. Note that the cross-sectional area of the liquid finger is assumed to be constant. The left-hand side of the equation accounts for the rate of change of momentum whereas the right-hand side includes all forces acting upon the control volume. The bracketed term on the left-hand side should in fact include a term proportional to the mass of the oil displaced by the water as it moves forward; however, inertia is found to be unimportant on observable time scales and so we make no effort here to incorporate an effective mass correction.

In Eq. (1), $f^{\mathrm{e}} = KV^2$ is the DEP force [1]. According to the assumption that the liquid profile is uniform along the length of the finger except at its leading edge, a simple electromechanical model may be used to determine that $K \propto \mathrm{d}C/\mathrm{d}Z$, where $C(Z)$ is the system capacitance, a function of the finger length. Because $C \propto Z(t)$, f^{e} is constant in time. This result is also obtained using a Maxwell stress tensor over the control volume [4]. The force of electrical origin f^{e} does not depend on the details of the field at the leading edge of the finger.

The surface tension term is $f_\gamma = -(\gamma_{\mathrm{L-L}})P_f$. Here, $\gamma_{\mathrm{L-L}}$ is the liquid–liquid interfacial tension between the oil bath and the water droplet. P_f, the perimeter of the oil–water interface, is assumed to remain constant as the liquid finger progresses. The surface tension term is roughly constant and retards the motion of the finger. The interfacial tension $\gamma_{\mathrm{L-L}}$ is here denoted simply as γ, so the expression for the force becomes, $f_\gamma = -\gamma P_f$. The fluid drag force $f_{\mathrm{d}} \approx -(P_f + 2w + g)Z(t)\tau_{\mathrm{d}}$ depends on the viscous shear stress τ_{d} which in turn is related to the finger velocity, $\mathrm{d}Z/\mathrm{d}t$, and the details of the velocity profile.

Eq. (1) can be simplified by recognizing that, even for the rapid transient flows we observe, the momentum term is insignificant on all important time scales and may be ignored. Note that both the electrical and surface tension forces are constant, and only the drag force depends on time. If we now assume,

$$\tau_{\mathrm{d}} = \mu_w G\frac{\mathrm{d}Z}{\mathrm{d}t}, \tag{2}$$

where μ_w is the dynamic viscosity of water, and G is a geometric parameter, the equation of motion reduces to,

$$\frac{\mathrm{d}Z^2}{\mathrm{d}t} = \frac{2(KV^2 - \gamma P_f)}{\mu_w G(P_f + 2w + g)}. \tag{3}$$

Applying the initial condition $Z(t = 0) = 0$, the solution is

$$Z(t) = A\sqrt{t}, \tag{4}$$

where

$$A = \sqrt{\frac{2(KV^2 - \gamma P_f)}{\mu_w G(P_f + 2w + g)}}. \tag{5}$$

Even lacking detailed knowledge of some of constants in Eq. (5) such as K, G, and P_f, most of the important parametric dependencies of A are evident. It should be noted that the same, simple "square-root" law, $Z(t) \propto \sqrt{t}$, arises in the description of certain capillary-driven flows that have compelling similarities to DEP microactuation [5].

Eq. (5) for A reveals a competition between the electrical and surface tension forces and predicts a minimum voltage required for forward movement: $V^* = \sqrt{\gamma P_f/K}$, that seems to be consistent with experimental observation. As long as the applied voltage V is comparable to V^*, we cannot expect a simple linear relationship between A and V. A linear relationship emerges only when the applied voltage $V \gg V^*$.

The values for all the parameters in Eq. (5) are readily available except K and G. K is a constant that accounts for the contributions from water and dielectric layer capacitances, respectively. An expression for K has been obtained by Jones et al. [6]. G is a geometric parameter dependent on the velocity profile of the finger. The oil film surrounding the water rivulet has a viscosity value much higher than water. Because of this viscous oil and the solid substrate underneath the extending finger, we have assumed that the velocity profile in our experiments resembles a Hagen–Poiseuille profile with no-slip boundary conditions. Another assumption is that the velocity of the finger is quasi steady. This assumption is adequate due to the low Reynold's number, $Re \sim 0.3$–3, but should eventually be tested with numerical simulations. Based on these assumptions, G can be determined from the shear stress exerted at the solid–liquid interface and it is a function of the width and gap of the electrode structure.

3.2. Experimental data

To study the finger dynamics, we have recorded the transient finger motion with a high-speed video camera. Typically, finger length data, $Z(t)$, were extracted from every 6th frame of videos recorded at 500 frames/s. The resulting data sets were analyzed using regression analysis based on the square-root law to yield values for A and associated confidence limits, based on Student's t-distribution statistics [7]. The continuous curve in Fig. 3 is the best-fit square-root law for the plotted data.

Table 1 compares values of the coefficient A_{calc}, obtained using known parameter values in Eq. (5), to experimental values, $A_{\mathrm{experiment}}$, obtained by least-squares regression

analysis of data as shown in Fig. 3. The trend with voltage is generally as expected but the correlation is not perfect. A possible explanation for the lack of close correlation is that our experiments are conducted at voltages fairly close to the threshold value for emergence of the finger. Our model, because it pertains to quasi-steady motion, rather than the initial formation of the finger, has not been successful in predicting this threshold. The motion of the finger in a $w = g = 20\,\mu m$ structure is sluggish at 200 V-rms, the voltage value we believe to be the threshold for finger formation. At 200 V-rms, the electrical force barely overcomes surface tension to actuate the finger. When the voltage is increased from 200 to 300 V-rms, the electrical force overwhelms surface tension and the least-squares estimates for $A_{experiment}$ increase significantly.

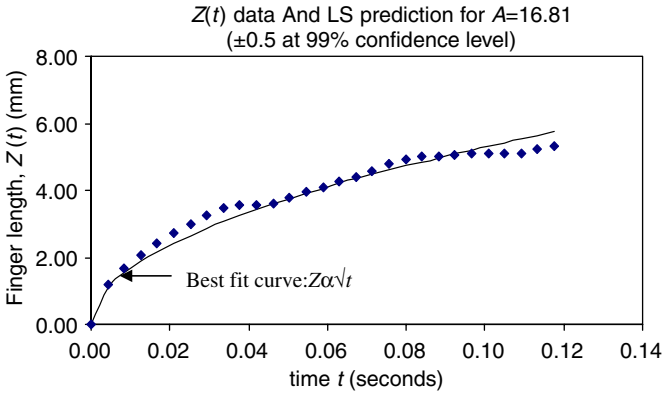

Fig. 3. Finger length $Z(t)$ versus time t for a 6 mm long structure with $w = 10$, $g = 20\,\mu m$. Applied voltage was 275 V-rms at 100 kHz. Structure had very small bumps to promote uniformly spaced droplet formation but these bumps had no effect on the transient dynamics.

3.3. Droplet formation dynamics

The rivulet becomes unstable immediately after voltage is removed. This instability is very much like the capillary jet instability familiar from ink-jet printers, flow cytometers, and liquid spraying. Several parameters are important in controlling the capillary instability and thus in determining the number of droplets formed. Most important is the total width of the electrode strips ($2w + g$), because it determines the wavelength of the capillary-driven instability.

For wide structures ($w = g = 50\,\mu m$), the instability must compete with the capillary force pulling the liquid back into the parent droplet. As a consequence of the return flow and reduced liquid inventory, fewer droplets form. For example, only one droplet, representing less than 30% of the original finger volume, is evident in Fig. 4a. For the somewhat narrower structure of Fig. 4b ($w = g = 20\,\mu m$), capillary instability progresses faster and breaks up the finger into six droplets including a satellite, totaling about 33% of the original finger volume. With still smaller structures ($w = 10, g = 20\,\mu m$), capillary instability breaks up the rivulet at even shorter wavelengths and the resulting

Table 1
Values of the coefficient A defined in Eq. (5) and computed from least-squares analysis of finger length $Z(t)$ versus time t data for co-planar electrode structures with $w = g = 20\,\mu m$

Applied voltage, V (V-rms)[a]	V^* (V-rms)	Frequency, f (kHz)	Dielectric coating	Least-squares $A_{experiment}$	Calculated A_{calc}
200	115	50	SU-8™	4.1±0.13	6.1
200	Same	50	Same	4.7±0.2	
225	Same	100	Same	4.6±0.4	7.3
300	Same	100	Same	12.1±1.5	10.4
300	Same	100	Same	12±1.0	
325	Same	100	Same	19.7±1.5	11.4
325	Same	100	Same	17.3±1.8	
375	Same	200	Same	17±2.9	13.4

The ± limits for $A_{Experimental}$ are obtained using Student's t-distribution statistics at the 99% confidence level.

[a]Probably due to variability in wetting conditions on the dielectric coatings, we have not been able to measure threshold voltage for finger formation reliably, but we are convinced that the values for the 20-μm structures tested are somewhere between 100 and 200 V-rms.

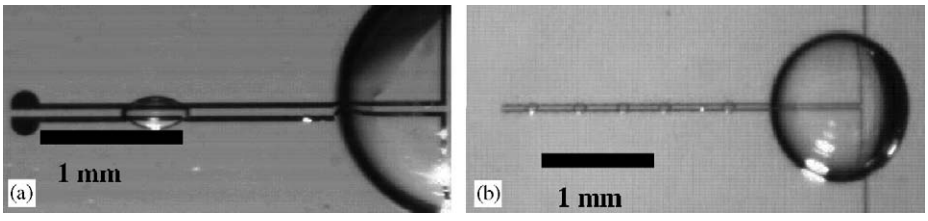

Fig. 4. Droplet formation in co-planar DEP structures. (a) Larger structure: $w = 50$, $g = 50\,\mu m$, length = 3 mm. (b) Smaller structure: $w = 20$, $g = 20\,\mu m$, length = 3 mm, with 6 droplets with average volume ~200 (S.D. = ±48) pL.

droplets contain more than 80% of the initial liquid rivulet volume.

4. More on capillary instability of a rivulet

Rayleigh's classical theory for the hydrodynamic instability of a cylindrical liquid jet of radius R in air predicts that disturbances at all wavelengths greater than $\lambda_c = 2\pi R$ are unstable, and that those at wavelength $\lambda^* = 9.016R$ will grow fastest [8]. Remarkably, this theory adequately predicts the spacing between droplets formed in our structures. To investigate the capillary instability of these static rivulets, we recorded the spacing and radii of the sessile droplets formed along the co-planar electrodes after voltage removal. Data have been obtained from electrode structures with the same cross-sectional dimensions used in the finger dynamics studies, viz., $w = 20$, $g = 20\,\mu m$ and $w = 10$, $g = 15$ and/or $20\,\mu m$. Fig. 5 shows an experiment conducted with a 6 mm long, narrow structure that produced ~30 droplets of average volume of ~40 pl (S.D. $= \pm 10$) at an average spacing of 160 (S.D. $= \pm 54$) μm. According to Rayleigh's theory, using $R = w + g/2$, the most unstable wavelength λ^* is 158 μm.

Experiments performed with structures covering a wide range of widths confirm that Rayleigh's inviscid, linear theory accurately predicts the droplet formation. However, one critical parameter ignored in this theory is viscosity. Weber accounted for the effect of liquid viscosity [9]. The modified most unstable wavelength, λ_{We}, has the following form:

$$\lambda_{We} = 2\pi R\sqrt{2 + 6(Oh/2)^{0.5}}, \quad (6)$$

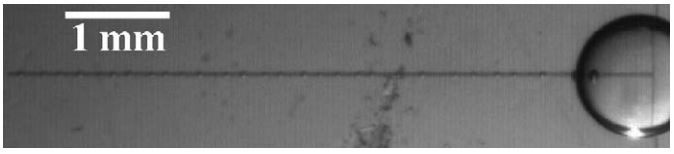

Fig. 5. Simultaneous formation of multiple droplets using an electrode structure with $w = 10$, $g = 15\,\mu m$, and length = 6 mm. Upon application of 400 V-rms at 100 kHz, the finger filled in <0.1 s. Approximately 30 droplets, of average volume of 40 (S.D. $= \pm 10$) pL and average spacing of 160 (S.D. $= \pm 54$) μm, were produced.

where Oh is the dimensionless Ohnesorge number,

$$Oh = \rho\upsilon^2/\gamma R, \quad (7)$$

where ρ, γ, υ, and R are density, interfacial tension, kinematic viscosity, and radius of the liquid, respectively. According to Eq. (7), in our experiments the effect of viscosity upon the most unstable wavelength λ^* is less than 3% for the case of deionized water.

Viscosity becomes more pronounced with liquids such as ethylene glycol, because υ increases by more than an order of magnitude to $\upsilon = 16.1$ cP. Using Eqs. (6) and (7), $\lambda^* = 532\,\mu m$ for ethylene glycol in a $w = 30$, $g = 30\,\mu m$ structure. This value is more than 30% larger than the value based on the inviscid model, i.e., $\lambda^* = 9.016R$. Difficulty in observing the progression of the instability for the case of ethylene glycol have precluded video recordings of droplet formation in this case; however, visual observations are consistent with the prediction that the wavelength is increased by the predicted amount.

5. Control of droplet spacing with periodic bumps

Droplet formation can be controlled using periodic semicircular bumps patterned on the co-planar electrodes, as shown in Fig. 6 [6], if the bumps are spaced according to Rayleigh's theory, i.e., $s = \lambda^* = 4.5(2w + g)$. Fig. 7(a) shows the result of an experiment with a structure with $w = 10\,\mu m$ and $g = 20\,\mu m$. One droplet has formed at each of the 21 bump sites on the surface. For this structure, the λ^* is about 200 μm. Fig. 7(b) demonstrates a similar experiment with a smaller structure: $w = 5$, $g = 10\,\mu m$. As in the previous case, we can see 21 droplets on 21 bumps plus a few irregulars at right where there are no bumps. For this structure, Rayleigh's theory predicts the most unstable wavelength to be 90 μm, while the bump spacing is about 100 μm. These results indicate that as long as the spacing is close to the most unstable value, precise formation of droplets is achieved. If the spacing between any two adjacent bumps is too large, satellite droplets form between them just as shown in Fig 4(b). Bumps have little or no influence on the wavelength of the capillary instability; instead, they merely initiate the instability in a regular fashion, leading to uniformly spaced and sized droplets.

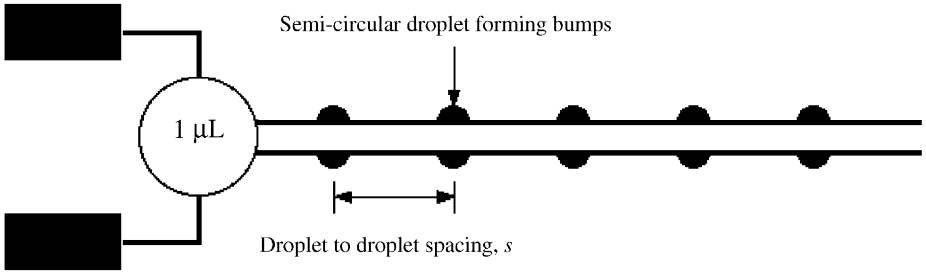

Fig. 6. Schematic representation of coplanar electrode strips with periodic semicircular bumps intended to fix the location of the droplets that form when the voltage is removed.

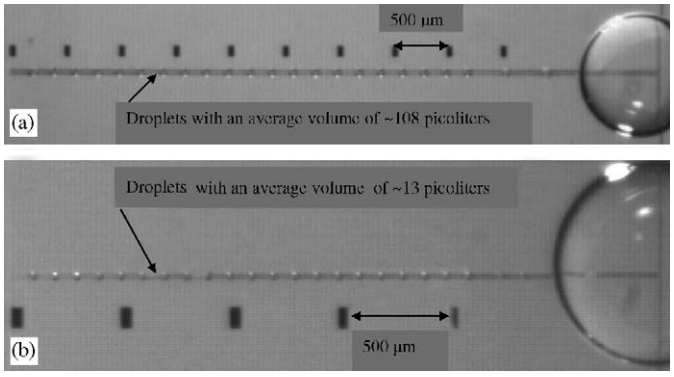

Fig. 7. Demonstration of the efficacy of placing periodic bumps on structures to produce equally spaced droplets. (a) Structure width is 10 μm and the gap is 20 μm. There are 21 droplets on exactly 21 bumps with an average volume of 108 pL. Two isolated droplets close to the parent droplet are formed due to the absence of bumps (b) Structure shape is identical to (a) with width of 5 μm and spacing of 10 μm. This frame also shows 21 droplets on the order of 13 pL on 21 bumps. Two isolated droplets are also visible.

Table 2
Electrode structures of different dimensions with estimated volumes of individual droplets

Electrode size (μm)	Finger diameter, $D = 2w+g$ (μm)	Measured droplet volume	Bump spacing (μm)	λ^* (μm)
$w = 50$ $g = 50$	150	~60 nL[a]	No bumps	676
$w = 20$ $g = 20$	60	~200 pL	No bumps	270.5
$w = 10$ $g = 20$	40	~100 pL	200	180
$w = 5$ $g = 10$	20	~10 pL	100	90

Reducing the total electrode width, $(2w+g)$ from 150 to 20 μm decreases droplet volume approximately three orders of magnitude.

[a]For the widest electrode structure, the droplet had the shape of a prolate spheroid, necessitating use of the volume equation for a prolate sphere, $V_d = (2/3)\pi ab^2$, where a and b are semi-major and semi-minor axes, respectively.

6. Droplet volume data

As long as the voltage is on, the finger maintains stable, static equilibrium of a cylinder with a semi-circular cross-section. When the voltage is removed, this equilibrium no longer exists, and the finger becomes unstable. With no electric field, two pressure terms act upon the water finger: the hydrostatic pressure of order ρgR, and the Laplace pressure of order γ/R. The dimensionless Bond number, $B_o = \rho gR^2/\gamma$, compares these terms and determines which one dominates [10]. For a 20-μm structure, $B_o < 10^{-3}$, indicating that the hydrostatic pressure is negligible and that the Laplace pressure term dominates. Driven by the Laplace pressure, the capillary instability progresses rapidly, breaking up the water finger into small droplets. The quantitative analysis presented here pertains to structures equal to or smaller than $w = g = 20\,\mu m$. In general, the resulting droplets are hemispherical in shape; thus

$$V_d = \frac{2}{3}\pi\left(\frac{D}{2}\right)^3. \quad (8)$$

Using Eq. (8) and estimates for D, the droplet diameter, we have determined the approximate volume of these droplets. Droplet volume scales as the 3rd power of the total electrode width $(2w+g)$, making it possible to create droplets as small as ~10 pL with the smallest structure ($w = 5$, $g = 10\,\mu m$) tested to date. Table 2 summarizes individual droplet volume and bump spacing data plus calculated values for λ^* for different electrode structures tested.

7. Conclusion

Liquid dielectrophoresis can be used to transport aqueous liquid volumes and to dispense regularly spaced, uniform droplets using co-planar electrodes formed on a dielectric-coated insulating substrate. The scheme has implications in novel microfluidic systems for the laboratory on a chip. When voltage is first applied, a finger of liquid emerges from a parent droplet and moves rapidly along the coplanar electrodes. When the finger reaches the end of the structure, it stops, having reached a new electrohydrostatic equilibrium. A simple theoretical model for the time-dependent finger motion predicts that the length $Z(t)$ is proportional to the square root of time, i.e., $Z \propto \sqrt{t}$. This predictive relation is reasonably successful in describing the motion.

When the voltage is removed, capillary instability breaks up the rivulet into regularly spaced droplets. Rayleigh's theory for the capillary instability of a cylindrical liquid jet successfully predicts the spacing of the droplets formed along the electrode structure. Accurate droplet dispensing is achieved using periodic bumps patterned on the co-planar electrodes. If these bumps are spaced at about the predicted most unstable wavelength λ^*, they initiate the instability and create droplets that are regularly spaced and equal in volume. Extensive experiments with structures of varied width demonstrate that the droplet dispenser is robust and reliable. The volume of the droplets scales as the 3rd power of the total electrode width $= 2w+g$. Uniform droplets as small as ~10 pL in volume are obtained with electrode structures of width 20 μm.

References

[1] R. Ahmed, T.B. Jones, C. Bailey, D. Hsu, Dispensing picoliter droplets using dielectrophoretic (DEP) microactuation, Microscale Thermophys. Eng. 8 (3) (2004) 271–283.
[2] T.B. Jones, J.R. Melcher, Phys. Fluids 16 (1973) 393–400.

[3] T.B. Jones, M.P. Perry, J.R. Melcher, Dielectric siphon, Science 174 (1971) 1232–1233.
[4] H.H. Woodson, J.R. Melcher, Electromechanical Dynamics, Part. 2, Wiley, New York, 1968 (Chapter 8).
[5] A.A. Darhuber, S.M. Trojan, W.W. Reisner, Dynamics of capillary spreading along hydrophilic microstripes, Phys. Rev. E 64 (2001) 031603.
[6] T.B. Jones, M. Gunji, M. Washizu, M.J. Feldman, Dielectrophoretic liquid actuation and nanodroplet formation, J. Appl. Phys. 89 (2) (2001).
[7] A.D. Rickmers, H.N. Todd, Statistics: An Introduction, McGraw-Hill, New York, 1967, (Chapter 12).
[8] J.W.S. Rayleigh, The Theory of Sound, vol. 2, Dover Publications, New York, 1945, pp. 359
[9] C. Weber, Zum Zerfall eines Flüssigkeitsstrahles, ZAMM 11 (1931) 135–154.
[10] P.-G. Gennes, F. Brochard-Wyart, D. Quere, Capillarity and Wetting Phenomena Drops, Bubbles, Pearls, Waves, Verlag, New York, 2004 (Chapter 1).